THE JOURNAL OF PHYSICAL CHEMISTRY A
A JOURNAL OF THE AMERICAN CHEMICAL SOCIETY

pubs.acs.org/JPCA

Article

Millimeter-Wave and High-Resolution Infrared Spectroscopy of 2-Furonitrile—A Highly Polar Substituted Furan

Brian J. Esselman, Maria A. Zdanovskaia, William H. Styers, Andrew N. Owen, Samuel M. Kougias, Brant E. Billinghurst, Jianbao Zhao, R. Claude Woods,* and Robert J. McMahon*

Cite This: *J. Phys. Chem. A* 2023, 127, 1909−1922

Read Online

ACCESS | Metrics & More | Article Recommendations | Supporting Information

ABSTRACT: The rotational spectrum of 2-furonitrile (2-cyanofuran) has been obtained from 140 to 750 GHz, capturing its most intense rotational transitions at ambient temperature. 2-Furonitrile is one of two isomeric cyano-substituted furan derivatives, both of which possess a substantial dipole moment due to the cyano group. The large dipole of 2-furonitrile allowed over 10 000 rotational transitions of its ground vibrational state to be observed and least-squares fit to partial octic, A- and S-reduced Hamiltonians with low statistical uncertainty (σ_{fit} = 40 kHz). The high-resolution infrared spectrum, obtained at the Canadian Light Source, allowed for accurate and precise determination of the band origins of its three lowest-energy fundamental modes (ν_{24}, ν_{17}, and ν_{23}). Similar to other cyanoarenes, the first two fundamental modes (ν_{24}, A″, and ν_{17}, A′, for 2-furonitrile) form an *a*- and *b*-axis Coriolis-coupled dyad. More than 7000 transitions from each of these fundamental states were fit to an octic A-reduced Hamiltonian (σ_{fit} = 48 kHz), and the combined spectroscopic analysis determines fundamental energies of 160.1645522 (26) cm^{-1} and 171.9436561 (25) cm^{-1} for ν_{24} and ν_{17}, respectively. The least-squares fitting of this Coriolis-coupled dyad required 11 coupling terms, G_a, G_a^J, G_a^K, G_a^{JJ}, G_a^{KK}, F_{bc}, F_{bc}^J, F_{bc}^K, G_b, G_b^J, and F_{ac}^K. Using both the rotational and high-resolution infrared spectra, a preliminary least-squares fit was obtained for ν_{23}, providing its band origin of 456.7912716 (57) cm^{-1}. The transition frequencies and spectroscopic constants provided in this work, when combined with theoretical or experimental nuclear quadrupole coupling constants, will provide the foundation for future radioastronomical searches for 2-furonitrile across the frequency range of currently available radiotelescopes.

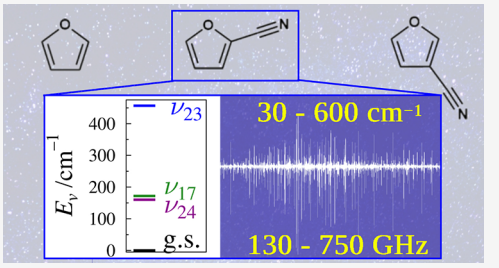

INTRODUCTION

Despite their prevalence in natural products, aromatic heterocycles with a permanent dipole moment have eluded all radioastronomical searches.[1−5] The feasibility of radioastronomical detection of a molecule depends upon its population in the source of interest, the intensity of its rotational transitions due to its dipole moment, and the quality of the measurements of its laboratory transition frequencies. The rotational spectrum[6−12] and high-resolution infrared spectrum of furan[13−15] have been well investigated, but, despite the available, high-quality laboratory spectra, this important heterocycle has eluded detection in the interstellar medium (ISM).[1,5,16] Furan (*c*-C_4H_4O, C_{2v}, κ = 0.916) is a near-oblate aromatic heterocycle with an *a*-axis dipole moment (μ_a = 0.661(6) D).[9] While its relatively weak permanent dipole moment makes the detection of furan more challenging, molecules with similar dipoles have been detected in extraterrestrial sources, *e.g.*, cyclopentadiene[17] and indene.[18]

Motivated by the recent detections of aromatic nitriles,[16,19−21] as well as the variety and abundance of nitrile-containing molecules detected in extraterrestrial sources,[22,23] we have investigated the rotational spectra of several six-membered ring aromatic and heteroaromatic nitriles, *i.e.*, benzonitrile,[24,25] three cyanopyridines,[26−28] cyanopyrimidine,[29] and cyanopyrazine.[30] The radioastronomical detections of benzonitrile[16,19] and cyanonaphthalenes[19,20] provide strong evidence for the existence of benzene and naphthalene in the ISM. Cyano substitution of benzene and naphthalene was critical to this conclusion, as neither parent species has a permanent dipole moment. The recent works on cyanoarenes may lead to the eventual detection of these species,[26−30] providing similarly strong evidence for the presence of their parent heterocycles (pyridine, pyrimidine, and pyrazine). To provide similar laboratory data for the astronomical community, we investigated the rotational spectra of the two regioisomeric furonitriles (cyanofurans) (Figure 1). Each of these species has a substantial increase in its dipole moment relative to furan, as a consequence of cyano substitution. Additionally, Simbizi *et al.* recently determined that the formation of furan, 2-furonitrile, and 3-furonitrile is thermodynamically favored in the conditions of the ISM.[31] For the first time, we present the rotational spectra and

Received: December 21, 2022
Revised: January 22, 2023
Published: February 16, 2023

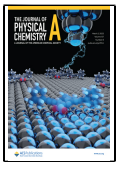

https://doi.org/10.1021/acs.jpca.2c08911
J. Phys. Chem. A 2023, 127, 1909−1922

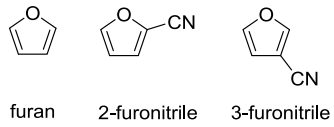

Figure 1. Furan and its two cyano-substituted derivatives, 2- and 3-furonitrile.

transition frequencies of 2-furonitrile. Our work with its regioisomer, 3-furonitrile, is ongoing and will be the subject of a future publication.

A unifying feature of the spectra of cyanoarenes is the *a*- and/or *b*-axis Coriolis-coupled dyad of their two lowest-energy fundamental states, the out-of-plane and in-plane vibrations of the nitrile group. As with these previous studies,[24−30] we report the rotational spectra of the ground vibrational state and the Coriolis-coupled dyad of the two lowest-energy fundamental vibrational modes (ν_{24} and ν_{17}). We also present a preliminary analysis of the third fundamental mode, ν_{23}. All three fundamental vibrations have been analyzed by high-resolution infrared spectroscopy, resulting in confirmation of the spectroscopic constants and precise determination of the band origins.

EXPERIMENTAL METHODS

A commercial sample of 2-furonitrile was used without purification for all spectroscopic measurements. Using a millimeter-wave spectrometer that has been previously described,[30,32,33] the rotational spectrum of 2-furonitrile was collected from 140 to 230 and from 235 to 750 GHz, in a continuous flow at room temperature, with sample pressures of 3−8 mTorr. The complete spectrum from 140 to 750 GHz was obtained automatically over ∼2 weeks given the following experimental parameters: 0.6 MHz/s sweep rate, 10 ms time constant, and 50 kHz AM and 500 kHz FM modulation in a tone burst design. A uniform frequency measurement uncertainty of 0.050 MHz was assumed for all measurements.

High-resolution infrared data presented in this work were recorded at the Canadian Light Source (CLS) Synchrotron Far-IR beamline (August 2022) using a Bruker IFS 125 HR Spectrometer, with synchrotron radiation and a 9.4 m optical pathlength difference providing a nominal resolution of 0.00096 cm^{-1}. The aperture was 1.15 mm, using a KBr beamsplitter, KBr cell windows, and a Ge:Cu detector, housed in a QMC cryogen-free cryostat (cooled by a Cryomech pulsed-tube cooler). The gain was set to 6×. The cell is a 2 m, White-type multipass cell; the total pathlength is 72 m. These spectra were obtained from 400 to 1200 cm^{-1} at a series of pressures for analysis of various vibrational states, which have substantially different infrared intensities. A uniform frequency measurement uncertainty of 0.00018 cm^{-1} (∼6 MHz) was assumed for all infrared measurements.

The separate segments of the rotational spectrum were combined into a single broadband spectrum using Kisiel's Assignment and Analysis of Broadband Spectra (AABS) software.[34,35] The AABS software suite was used to analyze both the rotational and high-resolution infrared spectra. Pickett's SPFIT/SPCAT[36] was used for least-squares fits and spectral predictions, along with Kisiel's PIFORM, PLANM, and AC programs for analysis.[37]

COMPUTATIONAL METHODS

Electronic structure calculations were carried out with Gaussian[38] using the WebMO interface[39] to obtain theoretical spectroscopic constants. Optimized geometries at the B3LYP/6-311+(2d,p) and MP2/6-311+(2d,p) levels were obtained using "verytight" convergence criteria and an "ultrafine" integration grid, and subsequent anharmonic vibrational frequency calculations were carried out. Additional electronic structure calculations were carried out using a development version of CFOUR[40] to obtain an optimized structure at the CCSD(T)/cc-pCVTZ level of theory. The optimized geometry and the same level of theory were subsequently used for anharmonic, second-order vibrational perturbation theory (VPT2) calculations, wherein cubic force constants are evaluated using analytical second derivatives at displaced points.[41−43] Computational output files can be found in the Supporting Information.

RESULTS AND DISCUSSION

Spectral Analysis. The recently expanded frequency range of our instrument allowed us to measure the rotational spectrum of 2-furonitrile up to 750 GHz,[30] a frequency coverage well beyond that used in some of our previous works on cyanoarenes (up to 375 GHz[24−27] or up to 500 GHz[28,29]). Spectral coverage up to 750 GHz is the nearly optimal range at ambient laboratory temperature (Figure 2), capturing nearly all of the most intense *a*- and *b*-type transitions for 2-furonitrile. The smaller size of the 2-furonitrile core reduces its mass and increases its rotational constants relative to the six-membered-ring cyanoarenes. The result of the smaller ring size and mass is twofold: an increased

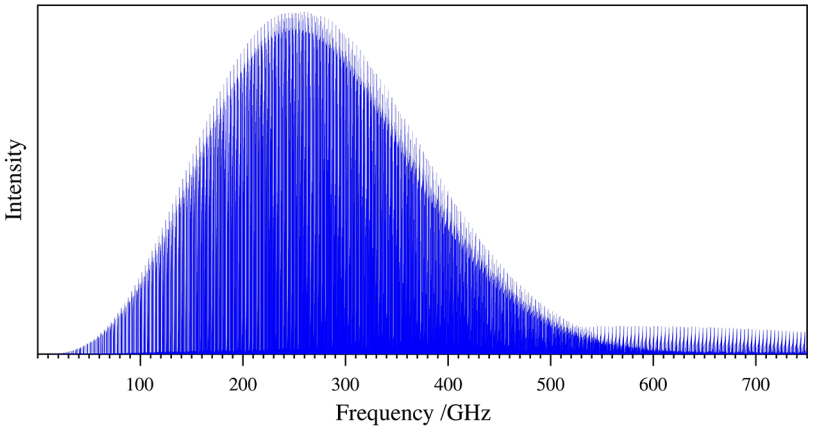

Figure 2. Predicted spectrum (SPCAT) of the ground vibrational state of 2-furonitrile to 750 GHz at 292 K.

https://doi.org/10.1021/acs.jpca.2c08911
J. Phys. Chem. A 2023, 127, 1909−1922

value of C_0 (~1663 MHz) leads to increased spacing of the low-K_a bands. The spectral coverage allows the observation of the K_a = 0 series transitions with a value of J'' + 1 = 42 near 140 GHz, increasing to J'' + 1 = 225 just below 750 GHz. Though the population of these transitions is quite small and the highest J'' + 1 of a K_a = 0 transition included in the data set is 190, the spectral range is comparable to that of cyanopyrazine.[30] This range of J'' + 1 (and the resulting range of K_a) quantum numbers provides a wealth of spectroscopic information on the centrifugal distortion and consequently necessitates a partial octic Hamiltonian to adequately model the spectrum.[30]

The ground-state rotational spectrum of 2-furonitrile (C_s, μ_a = 4.3 D, μ_b = 0.7 D, MP2; κ = −0.901) has not been previously investigated. The strong electron-withdrawing effect of the nitrile group, combined with the oxygen atom within the furan ring, results in a stronger *a*-axis and weaker *b*-axis dipole moment (Figure 3). The *a*-axis dipole is predominantly due to the nitrile

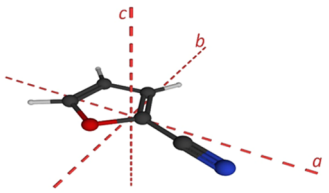

Figure 3. 2-Furonitrile (C_s, μ_a = 4.3 D, μ_b = 0.7 D; MP2) structure with principal inertial axes.

substituent, which lies very close to that axis. The *b*-axis dipole is similar in magnitude to the *a*-axis dipole of furan, 0.661(6) D.[9] The large difference in the *a*- and *b*-axis dipole components results in R-branch, *a*-type transitions (dominant in the spectrum below ca. 550 GHz) that are roughly 40 times more intense than the R-branch *b*-type transitions. As seen in Figure 2, when the intensity of the *a*-type transitions fades out at high values of J'' + 1, the spectrum consists predominantly of *b*-type R-branch transitions. Below 550 GHz, the rotational spectrum of 2-furonitrile is quite similar to the other cyanoarenes and is dominated by intense $^aR_{0,1}$ transitions, which form oblate-type band structures (Figure 4).

Ground-State Spectrum of 2-Furonitrile. For the ground vibrational state of 2-furonitrile, the spectral density and frequency range investigated allowed over 10 000 transitions to be measured, assigned, and least-squares fit (σ_{fit} = 34 kHz) to both S- and A-reduced Hamiltonians in the I^r representation. The resulting spectroscopic constants are provided in Table 1, along with their corresponding computed values. To adequately model the extensive data set (Figure 5), which ranged from J'' + 1 = 8 to 190 and K_a = 0 to 59, a near-complete octic Hamiltonian was required. Only the off-diagonal l_1 and l_{JJK} terms could not be determined in their respective reductions. Their values were held constant at zero, as no readily available computational software method has been implemented to estimate these terms. The B3LYP, MP2 (provided in Supporting Information Tables S2 and S3), and CCSD(T) spectroscopic constants are in excellent agreement with the experimental values. Fortuitously, the B3LYP calculations provide a closer estimate of the A_0, B_0, and C_0 values than the higher-level *ab initio* calculations. The B3LYP-computed rotational constants differ from the experimental values by less than 1.6 MHz (0.08%). The MP2 and CCSD(T) rotational constants differ from the experimental values by less than 0.6%. In contrast, the centrifugal distortion constants of 2-furonitrile are better predicted using either of the *ab initio* methods. The S-reduction CCSD(T) quartic distortion constants vary by less than 5% from the experimental values, with the exception of D_K, which has a 20% error. Similarly, all of the S-reduction CCSD(T) quartic distortion constants vary by less than 5%, with the exceptions of the two purely *J*-dependent terms H_J and h_J. As no previous experimental spectroscopic constants have been reported for 2-furonitrile, B3LYP-computed values were used to make *a priori* predictions of the rotational spectrum. These predictions were sufficient to identify and easily assign its transitions in the experimental spectrum.

Coriolis-Coupled Dyad of ν_{24} and ν_{17}. Similar to other cyanoarenes,[25−30] the lowest-energy fundamental modes of 2-furonitrile are the Coriolis-coupled, out-of-plane (ν_{24}, A″) and in-plane (ν_{17}, A′) bends of the nitrile group with large nitrogen-atom motions. The energy separations of these vibrations are all greater than 15 cm^{-1} for the cyanoarenes with six-membered rings, Table 2. In each of these cases, the lowest-energy

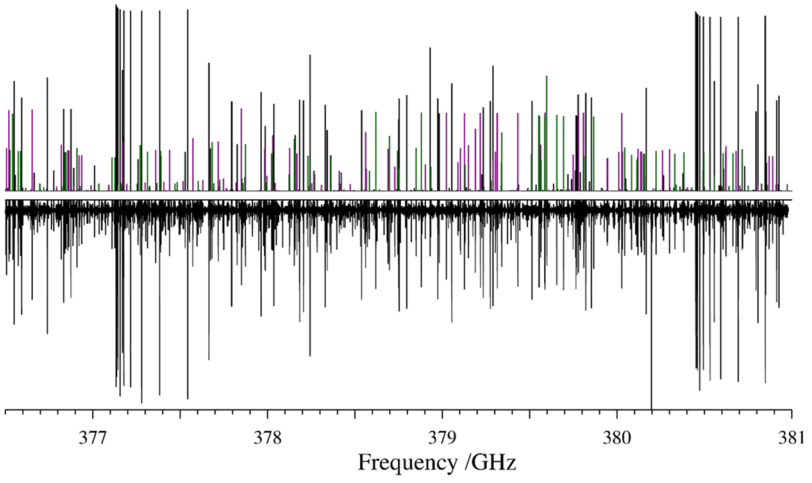

Figure 4. Predicted (top) and experimental (bottom) rotational spectra of 2-furonitrile from 376.5 to 381 GHz. The predicted ground-state spectrum, with prominent transitions for the J'' + 1 = 113 and J'' + 1 = 114 bands, appears in black. Transitions for ν_{24} are in magenta, and transitions for ν_{17} are in dark green. Unassigned transitions in the experimental spectrum are attributable to higher-energy vibrationally excited states of 2-furonitrile.

https://doi.org/10.1021/acs.jpca.2c08911
J. Phys. Chem. A 2023, 127, 1909−1922

Table 1. Experimental and Computational Spectroscopic Constants for the Ground Vibrational State of 2-Furonitrile (S- and A-Reduced Hamiltonian, I^r Representation)

	S reduction, I^r representation				A reduction, I^r representation		
	experimental	B3LYP[a]	CCSD(T)[b]		experimental	B3LYP[a]	CCSD(T)[b]
A_0 (MHz)	9220.25142 (10)	9220	9173	A_0 (MHz)	9220.25121 (10)	9220	9173
B_0 (MHz)	2029.274136 (17)	2031	2020	B_0 (MHz)	2029.277357 (17)	2031	2020
C_0 (MHz)	1662.643524 (17)	1664	1655	C_0 (MHz)	1662.640345 (17)	1664	1655
D_J (kHz)	0.0596802 (19)	0.0572	0.0568	Δ_J (kHz)	0.0796708 (19)	0.0757	0.0762
D_{JK} (kHz)	2.910358 (21)	2.75	2.89	Δ_{JK} (kHz)	2.790339 (21)	2.64	2.89
D_K (kHz)	0.29747 (20)	0.420	0.237	Δ_K (kHz)	0.39739 (20)	0.512	0.218
d_1 (kHz)	−0.01517569 (50)	−0.0144	−0.0144	δ_J (kHz)	0.01517638 (53)	0.0144	0.0144
d_2 (kHz)	−0.00999786 (30)	−0.00925	−0.00966	δ_K (kHz)	1.608947 (46)	1.50	1.63
H_J (Hz)	−0.000028009 (84)	−0.0000282	−0.00003220	Φ_J (Hz)	0.000009193 (91)	0.00000380	0.00000390
H_{JK} (Hz)	0.0045065 (17)	0.00386	0.00441	Φ_{JK} (Hz)	0.0066278 (65)	0.00571	0.00645
H_{KJ} (Hz)	−0.035910 (15)	−0.0315	−0.0363	Φ_{KJ} (Hz)	−0.043606 (26)	−0.0382	−0.0436
H_K (Hz)	0.03381 (16)	0.0292	0.0334	Φ_K (Hz)	0.03931 (16)	0.0340	0.0387
h_1 (Hz)	−0.000000851 (15)	−0.00000151	−0.00000180	ϕ_J (Hz)	0.000002606 (17)	0.00000163	0.00000170
h_2 (Hz)	0.000018831 (30)	0.0000160	0.0000180	ϕ_{JK} (Hz)	0.0033275 (43)	0.0029	0.00325
h_3 (Hz)	0.000003719 (13)	0.00000314	0.00000350	ϕ_K (Hz)	0.04928 (17)	0.04302	0.04786
L_J (mHz)	0.0000000173 (13)			L_J (mHz)	−0.0000000358 (15)		
L_{JJK} (mHz)	−0.000011414 (32)			L_{JJK} (mHz)	−0.00001420 (18)		
L_{JK} (mHz)	0.00015018 (50)			L_{JK} (mHz)	0.00011551 (72)		
L_{KKJ} (mHz)	−0.0015285 (40)			L_{KKJ} (mHz)	−0.0013964 (40)		
L_K (mHz)	0.001142 (44)			L_K (mHz)	0.001052 (44)		
l_{JJK} (mHz)	[0.]			l_J (mHz)	[0.]		
l_{JK} (mHz)	−0.00000003136 (69)			l_{JK} (mHz)	−0.000006118 (94)		
l_{KKJ} (mHz)	−0.00000000698 (45)			l_{KJ} (mHz)	−0.0000363 (49)		
l_K (mHz)	−0.00000000161 (12)			l_K (mHz)	[0.]		
Δ_i (uÅ^2)[c,d]	0.105059 (4)			Δ_i (uÅ^2)[c,d]	0.106034 (4)		
N_{lines}[e]	10143			N_{lines}[e]	10143		
σ_{fit} (MHz)	0.040			σ_{fit} (MHz)	0.040		

[a]Evaluated with the 6-311+G(2d,p) basis set. [b]Evaluated with the cc-pCVTZ basis set. [c]Inertial defect, $\Delta_i = I_c - I_a - I_b$. [d]Calculated using PLANM from the B_0 constants. [e]Number of fitted transition frequencies.

fundamental is the out-of-plane vibration, indicating a lower energy cost for the out-of-plane bending of the cyano substituent relative to the in-plane bend for these species. Neither of these vibrational modes was observed in the previous low-resolution, gas-phase infrared study of 2-furonitrile.[44] These two modes form a dyad of vibrational states that are well separated (Figure 6) from the vibrational ground state, the two-quanta vibrational states ($2\nu_{24}$, $\nu_{24}+\nu_{17}$, and $2\nu_{17}$), and the third fundamental mode (ν_{23}, A″). Due to the C_s symmetry of 2-furonitrile, ν_{24} and ν_{17} have both *a*- and *b*-axis Coriolis couplings. The initial predictions of the rotational spectra for ν_{24} and ν_{17} were made using the experimental ground-state rotational constants, computational vibration−rotation interaction constants, ground-state centrifugal distortion constants, and computed G_a and G_b Coriolis-coupling constants. A partial octic, Coriolis-coupled dyad Hamiltonian was employed, similar to our previous works involving analogous nitrile vibrational modes.[24−27,30,45,46] From this initial prediction and subsequent measurement, assignment, and least-squares fitting of the millimeter-wave data, spectroscopic constants were obtained, including an accurate and precise energy separation between ν_{24} and ν_{17}. This preliminary least-squares fit provided the foundation for the subsequent analysis of the high-resolution infrared spectrum obtained from CLS.

To determine the band origins for these modes, high-resolution infrared spectra were obtained at the Canadian Light Source. Similar to our previous study of benzonitrile,[24,25] the spectroscopic constants from the rotational spectrum allowed us to efficiently assign and least-squares fit transitions from the infrared spectrum. Analyzing the infrared spectra with rotational constants from a data set that had a broader range of J and K_a values than could be observed in the infrared spectrum was fortunate, as the infrared intensities of each mode are rather weak. The CCSD(T)-predicted integrated intensities of these vibrational transitions are 0.43 and 2.8 km/mol for ν_{24} and ν_{17}, respectively. As shown in Figure 7, the *c*-type infrared spectrum of ν_{24} is much weaker than the *a*- and *b*-type transitions of ν_{17}. Due to their relative intensities and close proximity in the IR spectrum with a $\Delta E_{24,17}$ value of 11.7791039 (36) cm^{-1}, the transitions of ν_{24} are almost completely obscured by the transitions of ν_{17}. With accurate and precise spectroscopic constants from a preliminary least-squares fit of the millimeter-wave transitions and computed transition dipoles, we were able to predict the infrared spectrum of ν_{24} such that only the band origin did not match the experimental spectrum. Use of Loomis−Wood plots allowed us to readily assign, measure, and least-squares fit the rotationally resolved transitions of ν_{17}, providing the ν_{17} band origin. With the $\Delta E_{24,17}$ value determined

https://doi.org/10.1021/acs.jpca.2c08911
J. Phys. Chem. A 2023, 127, 1909−1922

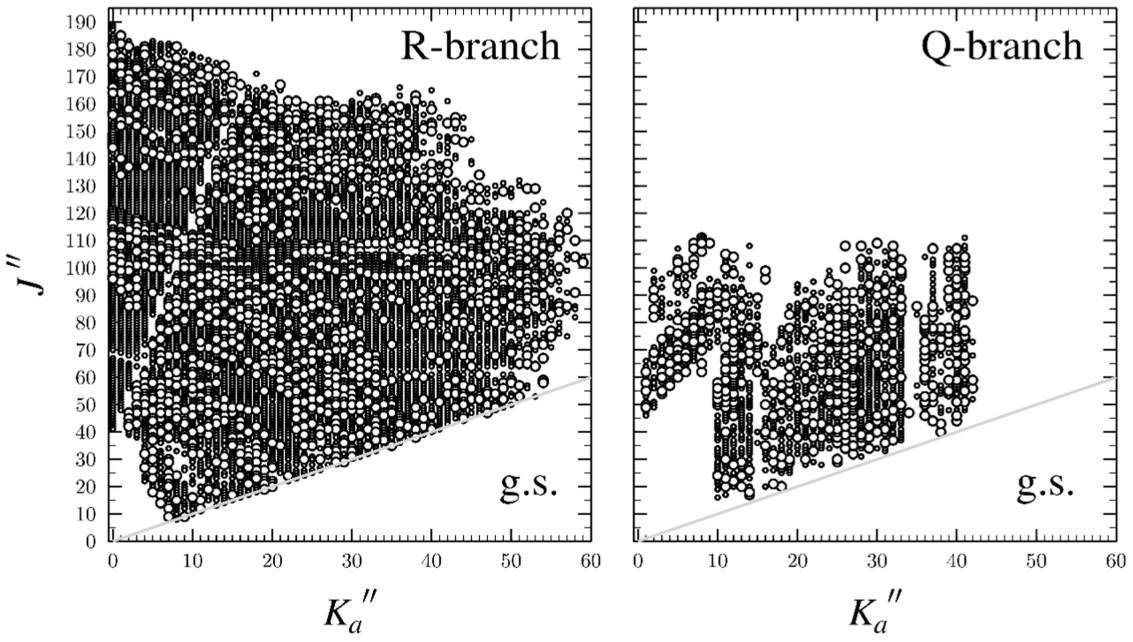

Figure 5. Data distribution plots for the least-squares fit of spectroscopic data for the vibrational ground state of 2-furonitrile. The size of the open circle is proportional to the value of $|(f_{obs.} - f_{calc.})/\delta f|$, where δf is the frequency measurement uncertainty, and all values are smaller than 3. The density of transitions is sufficiently large that many of the open circles are overlapping.

Table 2. Energy Difference Between Out-of-Plane and In-Plane Nitrile Bending Modes for Cyanoarenes

	out-of-plane	in-plane	ΔE (cm^{-1})
benzonitrile[24,25]	ν_{22}, B_1	ν_{33}, B_2	19.1081701 (74)
3-cyanopyridine[27]	ν_{30}, A″	ν_{21}, A′	15.7524693 (37)
4-cyanopyridine[26]	ν_{20}, B_1	ν_{30}, B_2	18.806554 (11)
2-cyanopyrimidine[29]	ν_{18}, B_1	ν_{27}, B_2	38.9673191 (77)
cyanopyrazine[30]	ν_{27}, A″	ν_{19}, A′	24.8245962 (60)
2-furonitrile (this work)	ν_{24}, A″	ν_{17}, A′	11.7791039 (36)

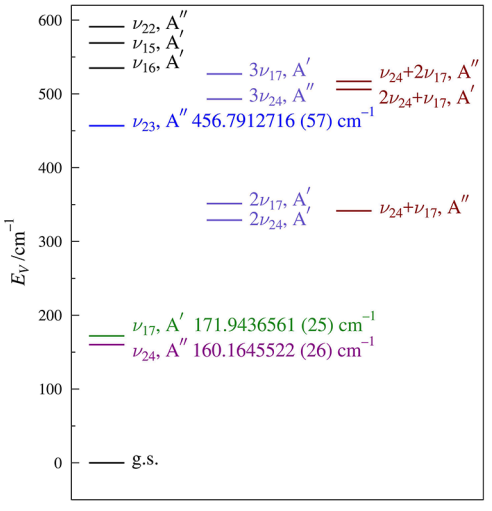

Figure 6. Vibrational energy levels of 2-furonitrile below 600 cm^{-1} from previous gas-phase experimental measurements[44] or extrapolated from their observed fundamentals. The energy values of ν_{24} (magenta), ν_{17} (dark green), and ν_{23} (blue) result from the experimental analysis of those vibrational states in this work. Energy levels of vibrational states not analyzed in this work are provided with fundamental states in black, overtone states in blue-gray, and combination states in dark red.

from the rotational transitions and the IR-determined band origin of ν_{17}, the weak transitions of ν_{24} were predicted within experimental error and readily assigned. Due to their weak intensity, however, very few ν_{24} transitions were obtained. The combined data set was least-squares fit using an octic A-reduced Hamiltonian in the I^r representation using SPFIT. The resulting spectroscopic constants are provided in Table 3 along with the ground-state spectroscopic constants for convenient comparison. Data set distribution plots showing both the rotational and infrared transitions included in the final data set are provided in Figures 8 and 9, respectively.

The final least-squares fit of the Coriolis-coupled dyad (ν_{24} and ν_{17}) contained over 7000 rotational transitions for each vibrational state, including many transitions involving energy levels perturbed by the interaction, many intensely shifted resonant transitions created by nearly degenerate energy levels of ν_{24} and ν_{17}, and 37 formally forbidden, coupling-allowed, nominal interstate transitions. A least-squares fit (A reduction, I^r representation) with a nearly complete set of sextic distortion constants for each vibrationally excited state (excluding Δ_K for ν_{17} and Φ_K and ϕ_K for both states) was obtained. This is a consequence of the broad range of quantum numbers of the transitions (11−185 in $J'' + 1$ and 0−52 in K_a for ν_{24}; 12−182 in $J'' + 1$ and 0−50 in K_a for ν_{17}) and the inclusion of many strongly perturbed transitions in the data set. Despite the presence of many *a*- and *b*-type transitions for each vibrationally excited state, the statistical uncertainties are quite large (480 kHz) for the values of A_{24} and A_{17}. The relatively poor determination of the *A* rotational constants and the inability to satisfactorily determine the *K*-dependent centrifugal distortion constants are related to the large *a*-axis Coriolis coupling that exists between these vibrationally excited states. Various combinations of *a*- and *b*-type coupling constants were employed to adequately model the observed rotational and infrared transitions. Despite the extensive data set, it was quite difficult to find a set of spectroscopic constants that would converge with low statistical uncertainty. In the end, the fit presented in this work includes 11

https://doi.org/10.1021/acs.jpca.2c08911
J. Phys. Chem. A 2023, 127, 1909−1922

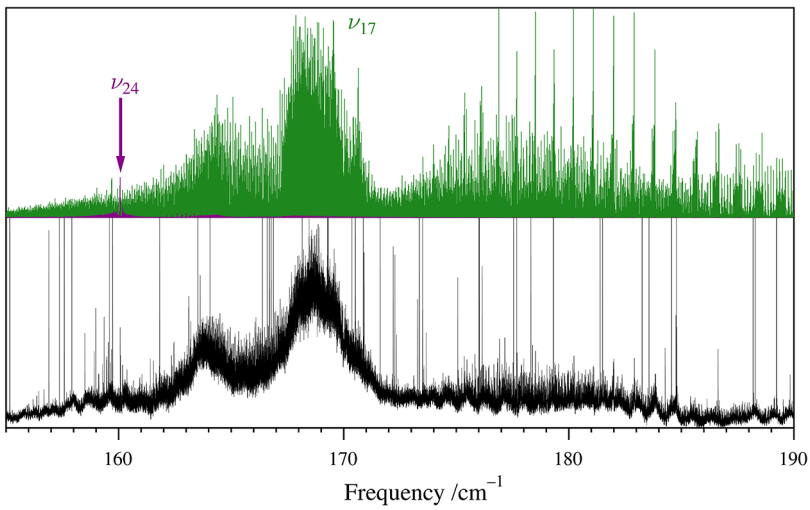

Figure 7. Predicted stick spectra of ν_{24} (magenta) and ν_{17} (dark green) of 2-furonitrile (top) and the experimental high-resolution infrared spectrum (bottom).

Table 3. Experimental Spectroscopic Constants for the Ground State and Vibrationally Excited States ν_{24} and ν_{17} of 2-Furonitrile (A-Reduced Hamiltonian, I^r Representation)

	ground state [a]	ν_{24} (A″, 165 cm^{-1}) [b,c]	ν_{17} (A′, 175 cm^{-1}) [b,c]
A_v (MHz)	9220.25121 (10)	9191.50 (48)	9245.93 (48)
B_v (MHz)	2029.277357 (17)	2032.346416 (38)	2034.134821 (41)
C_v (MHz)	1662.640345 (17)	1665.919974 (29)	1664.202091 (23)
Δ_J (kHz)	0.0796708 (19)	0.0814953 (14)	0.0820817 (15)
Δ_{JK} (kHz)	2.790339 (21)	2.6036 (22)	2.9241 (22)
Δ_K (kHz)	0.39739 (20)	0.537397 (77)	[0.39739]
δ_J (kHz)	0.01517638 (53)	0.01529931 (94)	0.01605486 (80)
δ_K (kHz)	1.608947 (46)	1.600359 (78)	1.646287 (80)
Φ_J (Hz)	0.000009193 (91)	0.000011397 (37)	0.000010956 (42)
Φ_{JK} (Hz)	0.0066278 (65)	0.0065838 (33)	0.0065356 (33)
Φ_{KJ} (Hz)	−0.043606 (26)	−0.04064 (12)	−0.04362 (12)
Φ_K (Hz)	0.03931 (16)	[0.03931]	[0.03931]
ϕ_J (Hz)	0.000002606 (17)	0.000003107 (23)	0.000003182 (21)
ϕ_{JK} (Hz)	0.0033275 (43)	0.0033629 (25)	0.0032475 (27)
ϕ_K (Hz)	0.04928 (17)	[0.04928]	[0.04928]
Energy (MHz)		4801612.479 (79)	5154741.130 (74)
Energy (cm^{-1})		160.1645522 (26)	171.9436561 (25)
G_a (MHz)		−14854.9 (56)	
G_a^J (MHz)		0.008393 (31)	
G_a^K (MHz)		0.02587 (88)	
G_a^{JJ} (MHz)		−0.000000017507 (51)	
G_a^{KK} (MHz)		−0.0000001666 (45)	
F_{bc} (MHz)		0.9065 (62)	
F_{bc}^J (MHz)		−0.000002636 (33)	
F_{bc}^K (MHz)		0.00004853 (12)	
G_b (MHz)		118.557 (59)	
G_b^J (MHz)		−0.00020718 (41)	
F_{ac}^K (MHz)		−0.00002775 (39)	
Δ_i (uÅ^2) [d,e]	0.106034 (4)	−0.2877 (29)	0.5677 (28)
N_{lines} rot [f]	10144	7388	7011
N_{lines} IR [f]		262	2727
σ_{fit} rot (MHz)	0.040	0.051	0.048
σ_{fit} IR (MHz)		2.1	2.8

[a]Ground-state constants reproduced from Table 1 for convenient comparison to those of ν_{24} (magenta) and ν_{17} (dark green). [b]Anharmonic vibrational frequency predicted using MP2/6-311+G(2d,p). [c]Constants that could not be experimentally determined, including those not explicitly shown, were held constant at the corresponding ground-state value. [d]Inertial defect, $\Delta_i = I_c - I_a - I_b$. [e]Calculated using PLANM from the B_0 constants. [f]Number of fitted transition frequencies.

https://doi.org/10.1021/acs.jpca.2c08911
J. Phys. Chem. A 2023, 127, 1909−1922

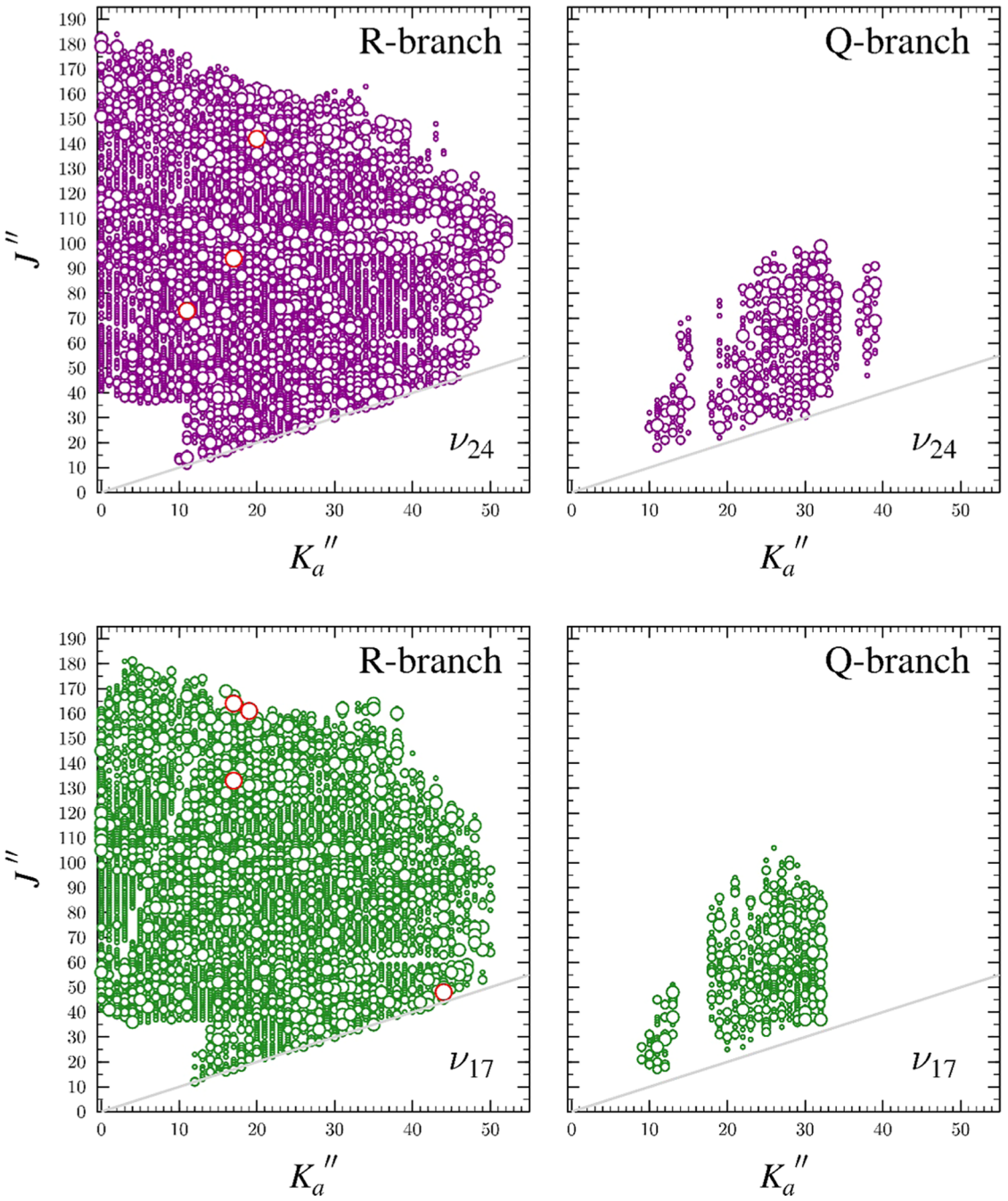

Figure 8. Data distribution plots for the least-squares fit of spectroscopic data for the pure rotational transitions of ν_{24} and ν_{17} of 2-furonitrile. The size of the open circle is proportional to the value of $|(f_{obs.} - f_{calc.})/\delta f|$, where δf is the assumed frequency measurement uncertainty of the rotational spectrum (0.050 MHz). There are only a limited number of transitions with such values greater than 3, and those are plotted in red, demonstrating that there is no systematic pattern of deviations from the assumed Hamiltonian.

Coriolis coupling coefficients (G_a, G_a^J, G_a^K, G_a^{JJ}, G_a^{KK}, F_{bc}, F_{bc}^J F_{bc}^K, G_b, G_b^J, and F_{ac}^K). Attempts to include F_{ac} in the least-squares fit were not successful. We were not able to remove many of the correlations between the spectroscopic constants. We were, however, able to obtain a satisfactory fit that reproduced the spectroscopic data, including the highly perturbed resonant transitions and the coupling-allowed nominal interstate transitions.

As shown in Table 4, there is excellent agreement between the computed vibration−rotation interaction constants (B_0−B_v and C_0−C_v) and their experimental values. Regardless of the level of theory (B3LYP, MP2, or CCSD(T)), the computed values agree within 0.2%, making them highly useful *a priori* predictive values when combined with the experimental ground-state constants. The A_0−A_v values do not show good agreement between theory and experiment, revealing the likely presence of untreated Coriolis coupling between ν_{24} and ν_{17} in both the experimental and computational values. These values show the tell-tale signs of untreated interactions between ν_{24} and ν_{17}, namely, large changes in the A_v rotational constant relative to the A_0 value with opposite signs and similar magnitudes for the two vibrationally excited states. The CCSD(T) values are highly perturbed, as the CFOUR algorithms do not deperturb the constants. Thus, these computed values are expected to be strongly impacted by the

https://doi.org/10.1021/acs.jpca.2c08911
J. Phys. Chem. A 2023, 127, 1909−1922

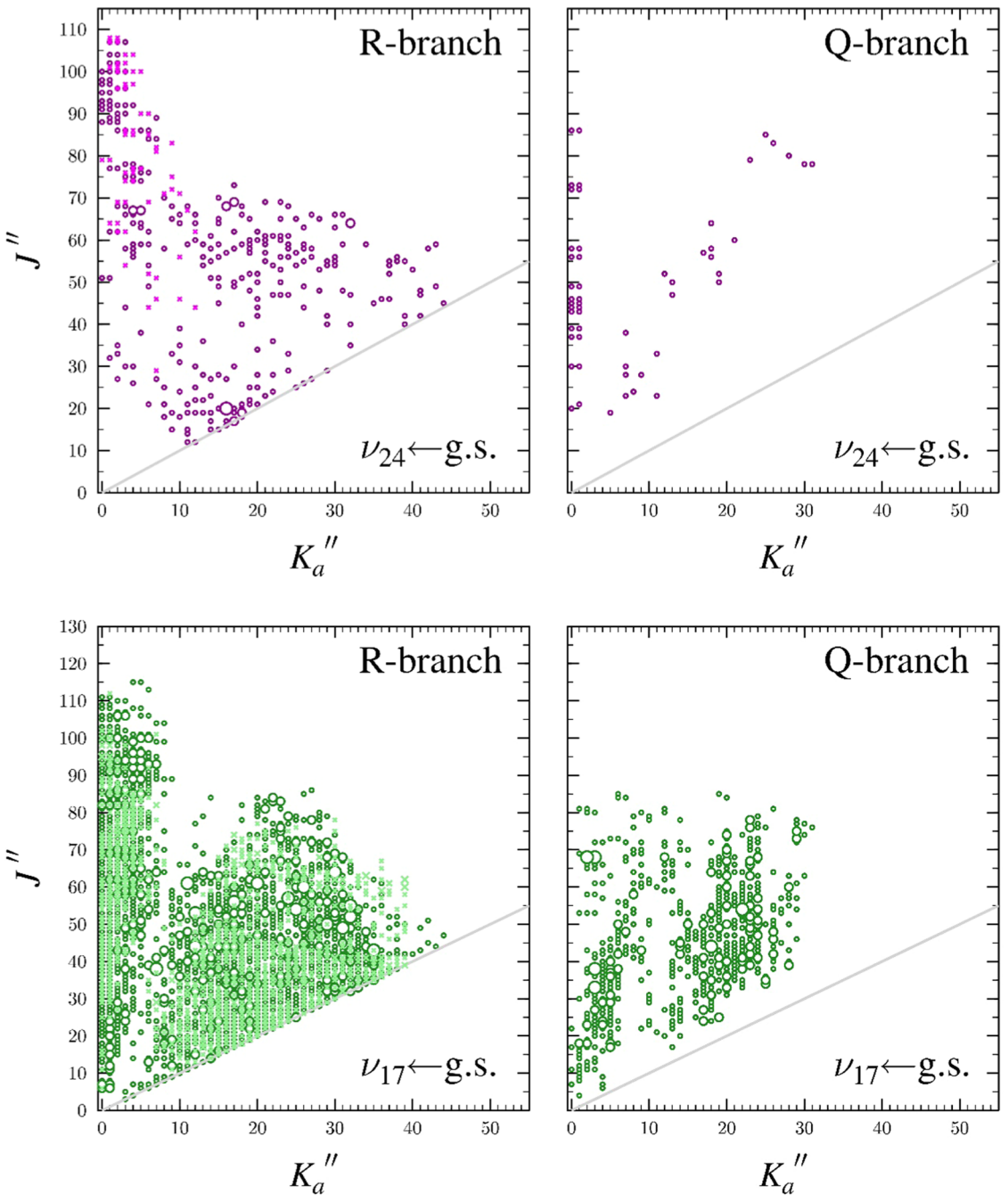

Figure 9. Data distribution plots for the least-squares fit of spectroscopic data for the rotationally resolved infrared transitions of ν_{24} and ν_{17} of 2-furonitrile. The size of the symbol is proportional to the value of $|(f_{obs.} - f_{calc.})/\delta f|$, where δf is the assumed IR frequency measurement uncertainty (6 MHz), and all values are smaller than 3.

large *a*-axis Coriolis coupling and a close agreement between the computed and experimental vibration−rotation interaction constants is not expected for ν_{24} or ν_{17} along the *a*-axis. This analysis is further supported by the close agreement between the average value of the vibration−rotation interaction constants (Table 4), which should remove the impact of untreated interactions between ν_{24} and ν_{17}. The average changes in the A_v rotational constants are in much closer agreement between theory and experiment for all three computational methods. Additionally, all three computational methods produce Coriolis zeta constants that are in good agreement with their experimental values, all of which would be adequate for initial predictions of the low-K_a series for each vibrationally excited state. The unscaled computed CCSD(T) band origins of ν_{24}, ν_{17}, and ν_{23} are too high by 1−2 cm^{-1}. The computed energy difference between ν_{24} and ν_{17} ($\Delta E_{24,17}$) differs from the experimental value determined in this work by only 0.6 cm^{-1}. A previous, low-resolution, gas- and liquid-phase, infrared and Raman study of 2-furonitrile identified two vibrational modes at 185 and 230 cm^{-1}.[44] Based upon the new measurements of the band origins of ν_{24} and ν_{17}, along with that of ν_{23} (*vide infra*), it is unclear what spectroscopic features were observed in the previous work.

Despite the aforementioned issues with the least-squares fit, the ability to model the frequencies of nominal interstate transitions or many transitions whose frequency is intensely

https://doi.org/10.1021/acs.jpca.2c08911
J. Phys. Chem. A 2023, 127, 1909−1922

Table 4. Vibration−Rotation Interaction and Coriolis-Coupling Constants of the ν_{24}-ν_{17} Dyad of 2-Furonitrile

	experimental	B3LYP[a]	MP2[a]	CCSD(T)[b]
A_0-A_{24} (MHz)	28.75 (48)	13.4	13.1	728.33
B_0-B_{24} (MHz)	−3.069059 (42)	−2.94	−3.01	−2.98
C_0-C_{24} (MHz)	−3.279629 (34)	−3.16	−3.22	−3.24
A_0-A_{17} (MHz)	−25.68 (48)	−10.5	−11.0	−725.65
B_0-B_{17} (MHz)	−4.857464 (44)	−4.61	−4.82	−4.86
C_0-C_{17} (MHz)	−1.561746 (29)	−1.46	−1.56	−1.56
A_0-A_{23} (MHz)	126.4341 (31)	133.5	125.2	130.061
B_0-B_{23} (MHz)	−1.39604 (80)	−1.19	−1.41	−1.38
C_0-C_{23} (MHz)	−1.69951 (66)	−1.16	−1.64	−1.64
$\frac{(A_0-A_{24})+(A_0-A_{17})}{2}$ (MHz)	1.54 (34)	1.49	1.05	1.34
$\frac{(B_0-B_{24})+(B_0-B_{17})}{2}$ (MHz)	−3.963262 (30)	−3.77	−3.92	−3.92
$\frac{(C_0-C_{24})+(C_0-C_{17})}{2}$ (MHz)	−2.420687 (22)	−2.31	−2.39	−2.40
$\lvert\zeta^a_{24,17}\rvert$	0.0806	0.812	0.817	0.815
$\lvert\zeta^b_{24,17}\rvert$	0.029	0.028	0.026	0.028
E_{24} (cm^{-1})	160.1645522 (26)	165.8	164.7	161.4
E_{17} (cm^{-1})	171.9436561 (25)	179.3	175.4	172.6
E_{23} (cm^{-1})	456.7912716 (57)	480.3	458.3	457.9
$\Delta E_{24,17}$ (cm^{-1})	11.7791039 (36)	13.5	10.6	11.2

[a]Evaluated with the 6-311+G(2d,p) basis set. [b]Evaluated with the cc-pCVTZ basis set.

perturbed by Coriolis interaction provides strong evidence that the system is otherwise well treated. Sharp *b*-type resonances are observed due to the mixing of ν_{24} and ν_{17} energy levels that are nearly degenerate, as shown in Figures 10−12. These sharp resonances are caused by a change in one of the energy levels associated with the resonant transition *via* Coriolis interaction. Typically, both energy levels experience a shift due to the global interaction and one level experiences a large shift associated with an energy-level crossing (as a function of J). The global interaction and the level crossings generally follow different ΔK selection rules. Figure 10 displays two intense *b*-type resonances ($\Delta K_a = 3$) at $J'' + 1 = 77$ and 109 for the $K_a = 15^+$ series of ν_{24} and the $K_a = 12^+$ series of ν_{17}, respectively. These resonant transitions are displaced from their unperturbed frequencies by about 1.3 and 2 GHz, respectively. *b*-Type resonances dominate the spectrum between the $K_a{}^+$ series of ν_{24} and ν_{17}. As shown in Figures 11 and 12, the sharp resonances are accompanied by large undulations that progress to higher $J'' + 1$ values as a function of K_a. The sharp resonances, sets of a few transitions with highly perturbed frequencies, are created by intense state mixing that is localized to a few values of J'', caused by a large shift in one of the energy levels associated with the transition. The resonances grow in intensity and likewise move to progressively higher $J'' + 1$ values as a function of K_a. The large undulations shown in these series of constant K_a transitions are caused by changes in both the spectroscopic constants between the ground and vibrationally excited states and the Coriolis coupling. These undulations result in transitions with highly perturbed frequencies that gradually change as a function of J'' rather than being localized to a few values of J''. Initial fitting of these undulations provides refinement of both types of spectroscopic constants, but many of the sharp local resonances

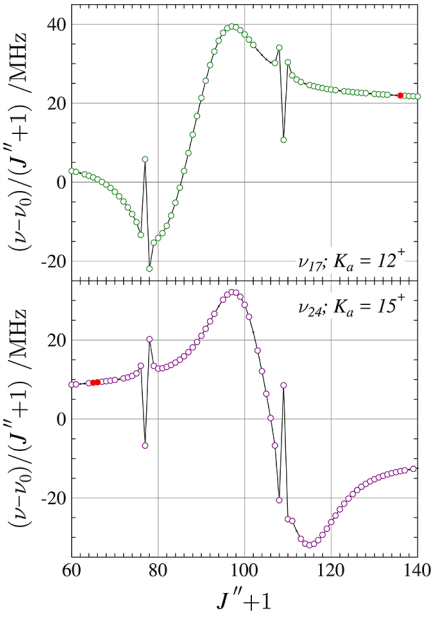

Figure 10. Resonance plots for 2-furonitrile showing the $K_a = 15^+$ series for ν_{24} and the $K_a = 12^+$ series for ν_{17}. These two resonances conform to the $\Delta K_a = 3$ selection rule for *b*-type resonances. The plotted values are frequency differences between excited-state transitions and their ground-state counterparts ($\nu - \nu_0$), scaled by ($J'' + 1$) to make the plots more horizontal. Measured transitions are represented by circles: ν_{24} (magenta), ν_{17} (dark green). Red circles indicate transitions whose *obs.* − *calc.* value exceeds 150 kHz. Predictions from the final coupled fit are represented by a solid, black line.

https://doi.org/10.1021/acs.jpca.2c08911
J. Phys. Chem. A 2023, 127, 1909−1922

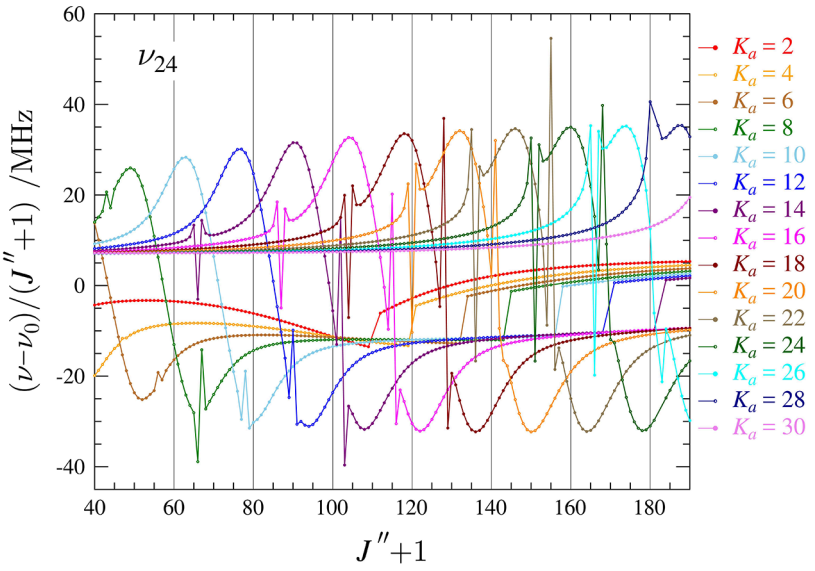

Figure 11. Superimposed resonance plots of ν_{24} for $^aR_{0,1}$ even-K_a^+ series from 2 to 30 for 2-furonitrile. Measured transitions are omitted for clarity, but they are indistinguishable from the plotted values on this scale. The plotted values are frequency differences between excited-state transitions and their ground-state counterparts $(\nu - \nu_0)$, scaled by $(J'' + 1)$.

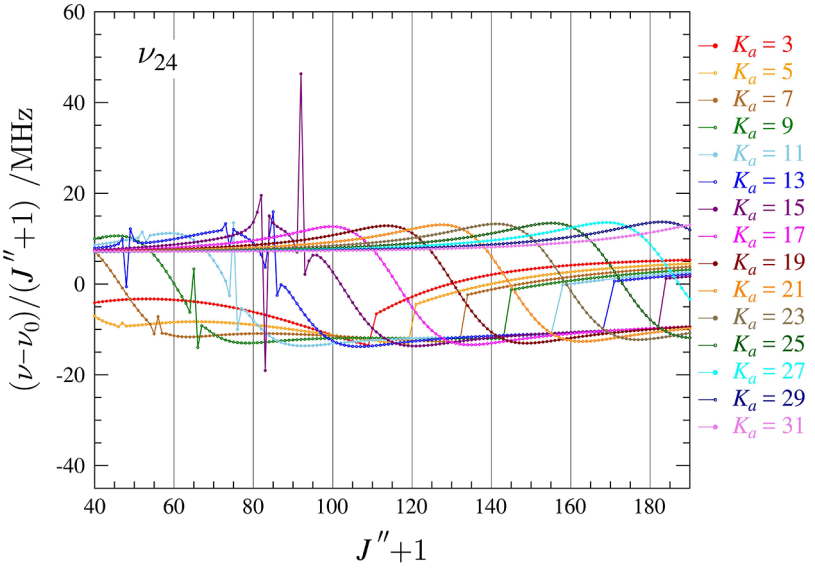

Figure 12. Superimposed resonance plots of ν_{24} for $^aR_{0,1}$ odd-K_a^- series from 3 to 31 for 2-furonitrile. Measured transitions are omitted for clarity, but they are indistinguishable from the plotted values on this scale. The plotted values are frequency differences between excited-state transitions and their ground-state counterparts $(\nu - \nu_0)$, scaled by $(J'' + 1)$.

need to be included in the fit to determine precise values of the coupling coefficients and the energy separation between the two vibrationally excited states.

As evidenced in the higher $J'' + 1$ region of the resonance progression plots of Figures 11 and 12, the intense state mixing also causes SPFIT/SPCAT to change the state labels on the K_a series, resulting in the observed discontinuities. Transitions near or at the discontinuity were often excluded from the least-squares fitting, for convenience, as their quantum number assignments were not stable. While these frequencies are correctly assigned and can be predicted within the experimental uncertainty to transitions of the coupled dyad, the intense state mixing makes their quantum number assignments ambiguous. Given the very large data set, removal of these transitions had no noticeable negative impact on the least-squares fit.

The aforementioned resonances and discontinuities are due to the state mixing caused by the Coriolis coupling between ν_{24} and ν_{17}, which causes observably intense coupling-allowed nominal interstate transitions. These formally forbidden, nominal interstate rotational transitions are observable from the energy levels with the most intense state mixing, which often correspond to the energy levels involved in the most perturbed transition frequencies. An example of a set of nominal interstate transitions and their in-state counterparts is illustrated in Figure 13. These nominal interstate transitions share energy levels with the in-state resonant transitions; thus, the average of the interstate and intrastate transitions must be identical. In the case of the transitions depicted in Figure 13, the frequency averages agree to a fortuitously low value of 1 kHz. The inclusion of the many *b*-type resonant transitions and the nominal interstate

https://doi.org/10.1021/acs.jpca.2c08911
J. Phys. Chem. A 2023, 127, 1909−1922

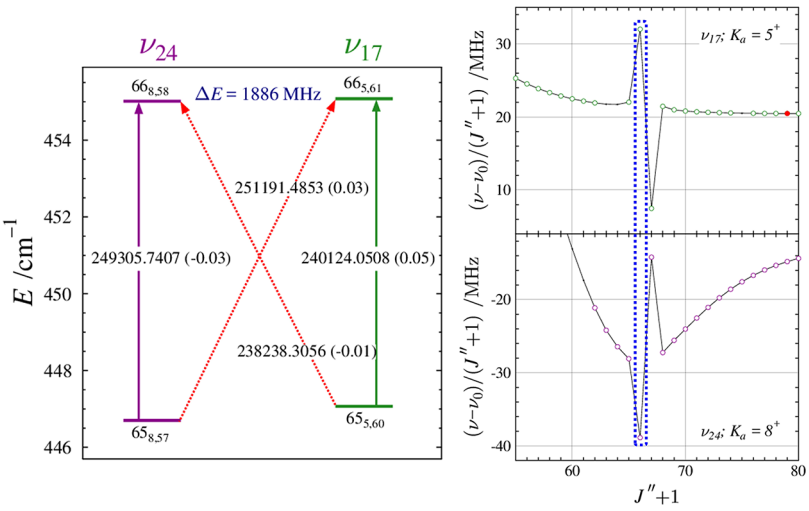

Figure 13. Energy diagram (left) depicting a representative matched pair of nominal interstate transitions between the ν_{24} (magenta) and ν_{17} (dark green) vibrational states of 2-furonitrile. Standard $^qR_{0,1}$ transitions within vibrational states are denoted by vertical arrows. The diagonal, dashed arrows indicate nominal interstate transitions that are formally forbidden, but enabled as a result of rotational energy-level mixing. Values printed on each of the arrows are the corresponding transition frequency (in MHz) with its *obs.* − *calc.* value in parentheses. The marked energy separation is between the two strongly interacting rotational energy levels. Resonance plots (right) of the K_a series of ν_{24} and ν_{17} that contain the corresponding resonant transitions identified with a blue box.

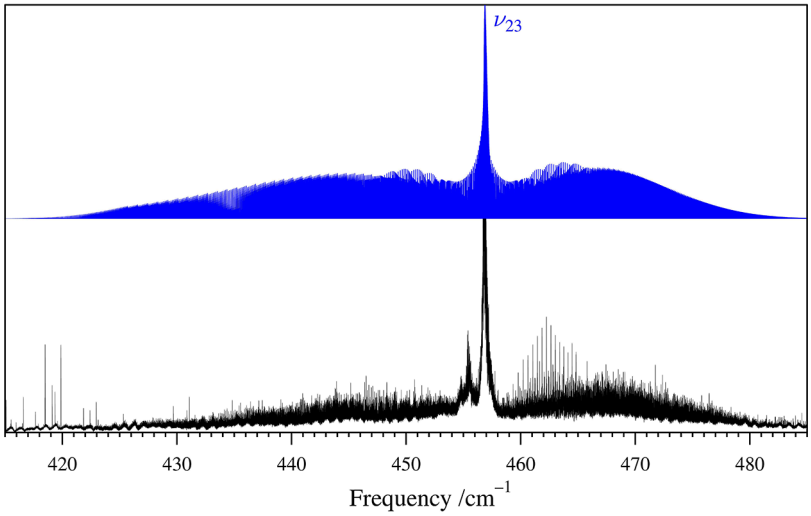

Figure 14. Predicted stick spectrum of ν_{23} (blue) of 2-furonitrile (top) and the experimental high-resolution infrared spectrum (bottom). Rotationally resolved, infrared transitions for hot bands associated with ν_{23} are visible in the experimental spectrum, including the large Q-branches clearly visible at slightly lower frequencies than the Q-branch of ν_{23}.

transitions provides a very substantial constraint on the $\Delta E_{24,17}$ value and the Coriolis coupling values. Thus, we are confident that the spectroscopic constants, including at least the lower-order Coriolis coupling terms, are well determined and likely to be physically meaningful, with the exception of the ambiguity regarding the A_v constants. While there may be other least-squares fits possible from this set of data, the presented constants are likely to be predictive of transitions of somewhat higher frequency and also substantially lower frequency.

Coupled Triad of $2\nu_{24}$, $\nu_{24}+\nu_{17}$, and $2\nu_{17}$. Within the vibrational energy manifold of 2-furonitrile (Figure 6), the next lowest-energy vibrationally excited states are the overtone and combination states ($2\nu_{24}$, $\nu_{24}+\nu_{17}$, and $2\nu_{17}$) centered at about 340 cm^{-1}. These states form a Coriolis- and Darling−Dennison-coupled triad similar to that observed for benzonitrile.[25] The excellent fit of the ground vibrational state and the Coriolis-coupled dyad of ν_{24} and ν_{17} provides a strong indicator that modeling of the transitions of this triad does not require treatment of interactions with the lower-energy vibrationally excited states. The energy separation of ∼150 cm^{-1} between the dyad and triad is sufficient for these states to prevent strong interactions between them. It is likely that these three states can be modeled as a triad, given that the next fundamental, ν_{23}, lies ∼100 cm^{-1} higher in energy, but we cannot entirely preclude a significant interaction between ν_{23} and the triad. Though beyond the scope of this work, the measurement, assignment, and least-squares fitting of these states are underway, facilitated using extrapolated spectroscopic constants from the ground state, ν_{24}, and ν_{17} and known relationships between the dyad and triad Coriolis-coupling terms and other parameters.

Vibrational Modes from 450 to 600 cm^{-1}, ν_{23}, $3\nu_{24}$, $2\nu_{24}+\nu_{17}$, $\nu_{24}+2\nu_{17}$, $3\nu_{17}$, ν_{16}, ν_{15}, and ν_{22}. The third

https://doi.org/10.1021/acs.jpca.2c08911
J. Phys. Chem. A 2023, 127, 1909−1922

Table 5. Experimental Spectroscopic Constants for Ground State and Vibrationally Excited State ν_{23} of 2-Furonitrile (A-Reduced Hamiltonian, I^r Representation)

	ground state [a]	ν_{23} (A″, 458 cm^{-1}) [b,c]
A_v (MHz)	9220.25121 (10)	9093.8171 (31)
B_v (MHz)	2029.277357 (17)	2030.673396 (80)
C_v (MHz)	1662.640345 (17)	1664.339855 (66)
Δ_J (kHz)	0.0796708 (19)	0.0802076 (58)
Δ_{JK} (kHz)	2.790338 (21)	2.77858 (32)
Δ_K (kHz)	0.39739 (20)	−5.646 (18)
δ_J (kHz)	0.01517638 (53)	0.0153073 (31)
δ_K (kHz)	1.608947 (46)	1.36501 (33)
Φ_J (Hz)	0.000009193 (91)	0.00000609 (29)
Φ_{JK} (Hz)	0.0066278 (65)	0.005861 (25)
Φ_{KJ} (Hz)	−0.043606 (26)	−0.03773 (69)
Φ_K (Hz)	0.03931 (16)	1.598 (28)
ϕ_J (Hz)	0.000002606 (17)	[0.000002606]
ϕ_{JK} (Hz)	0.0033275 (43)	[0.0033275]
ϕ_K (Hz)	0.04928 (17)	[0.04928]
Energy (MHz)		13694257.81 (17)
Energy (cm^{-1})		456.7912716 (57)
Δ_i (uÅ^2) [d,e]	0.106034 (4)	−0.795205 (24)
N_{lines} rot [f]	10144	790
N_{lines} IR [f]		1979
σ_{fit} rot (MHz)	0.040	0.043
σ_{fit} IR (MHz)		3.1

[a]Ground state (black) constants reproduced from Table 1 for convenient comparison to those of ν_{23} (blue). [b]Anharmonic vibrational frequency predicted using MP2/6-311+G(2d,p). [c]Constants that could not be experimentally determined, including those not explicitly shown, were held constant at the corresponding ground-state value. [d]Inertial defect, $\Delta_i = I_c - I_a - I_b$. [e]Calculated using PLANM from the B_0 constants. [f]Number of fitted transition frequencies.

fundamental, ν_{23} (A″, 457 cm^{-1}),[44] is an out-of-plane C−C−N bending mode of the cyano substituent with large amplitude motion of the central carbon atom and a smaller amplitude out-of-plane ring deformation. With rotational transitions about 10% as intense as those of the ground state, transitions for ν_{23} were readily assigned using the ground-state rotational constants and the computed vibration−rotation interaction constants. The ν_{23} band consists of *c*-type infrared transitions (Figure 14) predicted to be nearly as intense as ν_{17}, allowing the infrared transitions to be readily assigned from spectroscopic constants determined *via* its rotational spectrum. It quickly became clear that the transitions could not be fully treated with a single-state Hamiltonian model, due to coupling interactions with near-energy states. Fundamental ν_{23} has expected *a*- and *b*-axis Coriolis interactions with ν_{16} (A′, 535 cm^{-1}),[44] $|\zeta^a_{23,16}| = 0.934$ and $|\zeta^b_{23,16}| = 0.006$ (CCSD(T)). Fundamental ν_{16} may also have significant Coriolis interactions with ν_{22} and ν_{15}, though the computed $|\zeta^x_{22,16}|$, $|\zeta^c_{16,15}|$, and $|\zeta^x_{22,15}|$ values are much smaller. There may be additional interactions with the nearby tetrad of ν_{24} and ν_{17} three-quanta states, but this interaction is less likely due to the large changes in energy-level quantum numbers. In light of the complexity of these interactions, we present only a preliminary analysis of ν_{23} in this work, which provides effective spectroscopic constants and an accurate and precise band origin but does not treat any coupling interactions.

The effective A-reduction spectroscopic constants of ν_{23} in the I^r representation determined from a combined data set of rotational and infrared transitions are provided in Table 5. A data set distribution plot can be found in the Supporting Information for ν_{23}. To obtain a reasonable effective fit, many observed transitions were excluded from the data set. Despite the effective nature of the fit, there is generally good agreement between the computed vibration−rotation interaction constants and their experimental values (Table 4). All of the computed and experimental A_0-A_{23} values exceed 125 MHz, indicating that they are likely to reflect untreated Coriolis interactions with ν_{16}. This interpretation is corroborated by the similarly large and opposite-signed CCSD(T) computed value of A_0-A_{16} of −129 MHz. There is also generally good agreement between the centrifugal distortion constants of the ground state and ν_{23}, with the notable exceptions of the on-diagonal, *K*-dependent terms (Δ_K and Φ_K). The experimental value of Δ_K for ν_{23} is larger by an order of magnitude and of the opposite sign than its ground-state counterpart. This relationship is not surprising, as the untreated *a*-axis coupling between ν_{23} and ν_{16}, as well as any potential interactions with other nearby vibrational states, are being absorbed by A_{23} and the *K*-dependent centrifugal distortion constants. The experimental value of Φ_K for ν_{23} is larger by 2 orders of magnitude than the ground-state value. Attempts to fix these terms at their ground-state values resulted in high-error least-squares fits or resulted in the removal of many hundreds of transitions from the data set. Despite these limitations of the presented one-state fit, we are confident that the band origin of ν_{23} is precise and accurate.

CONCLUSIONS

Considering the prevalence of nitrile-substituted species among those that have been detected extraterrestrially and the

https://doi.org/10.1021/acs.jpca.2c08911
J. Phys. Chem. A 2023, 127, 1909−1922

likelihood of nitrile-substituted species being present in highly nitrogen-rich environments, *e.g.*, Saturn's moon, Titan, the acquisition and analysis of laboratory spectra of various cyano-substituted species is an important effort. Such molecules have already proven useful in serving as tracer molecules for parent species with smaller or nonexistent permanent dipole moments, *e.g.*, benzene and benzonitrile. Furan has thus far eluded detection in the interstellar medium. The spectroscopic constants and transition frequencies for 2-furonitrile presented in this work now allow it to serve as a potential tracer molecule for its less polar parent compound in extraterrestrial environments.

■ ASSOCIATED CONTENT

Supporting Information

The Supporting Information is available free of charge at https://pubs.acs.org/doi/10.1021/acs.jpca.2c08911.

Data set distribution plots for millimeter-wave and IR data for vibrationally excited state ν_{23} of 2-furonitrile, experimental and computed state spectroscopic constants for the vibrational ground state of 2-furonitrile in both A and S reduction (PDF)

Computational output files, least-squares fitting files for all vibrational states (ZIP)

■ AUTHOR INFORMATION

Corresponding Authors

R. Claude Woods − *Department of Chemistry, University of Wisconsin−Madison, Madison, Wisconsin 53706, United States;* orcid.org/0000-0003-0865-4693; Email: rcwoods@wisc.edu

Robert J. McMahon − *Department of Chemistry, University of Wisconsin−Madison, Madison, Wisconsin 53706, United States;* orcid.org/0000-0003-1377-5107; Email: robert.mcmahon@wisc.edu

Authors

Brian J. Esselman − *Department of Chemistry, University of Wisconsin−Madison, Madison, Wisconsin 53706, United States;* orcid.org/0000-0002-9385-8078

Maria A. Zdanovskaia − *Department of Chemistry, University of Wisconsin−Madison, Madison, Wisconsin 53706, United States;* orcid.org/0000-0001-5167-8573

William H. Styers − *Department of Chemistry, University of Wisconsin−Madison, Madison, Wisconsin 53706, United States;* orcid.org/0000-0002-8382-0180

Andrew N. Owen − *Department of Chemistry, University of Wisconsin−Madison, Madison, Wisconsin 53706, United States;* orcid.org/0000-0001-5903-1651

Samuel M. Kougias − *Department of Chemistry, University of Wisconsin−Madison, Madison, Wisconsin 53706, United States;* orcid.org/0000-0002-9877-0817

Brant E. Billinghurst − *Canadian Light Source. Inc., University of Saskatchewan, Saskatoon, Saskatchewan S7N 2V3, Canada;* orcid.org/0000-0002-5346-5317

Jianbao Zhao − *Canadian Light Source. Inc., University of Saskatchewan, Saskatoon, Saskatchewan S7N 2V3, Canada;* orcid.org/0000-0003-3864-2167

Complete contact information is available at: https://pubs.acs.org/10.1021/acs.jpca.2c08911

Notes

The authors declare no competing financial interest.

■ ACKNOWLEDGMENTS

We gratefully acknowledge funding from the U.S. National Science Foundation for support of this project (CHE-1664912 and CHE-1954270). We thank Michael McCarthy for the loan of an amplification-multiplication chain and the Harvey Spangler Award (to B.J.E.) for funding that supported purchase of the corresponding detector. Part of the research described in this paper was performed at the Canadian Light Source, a national research facility of the University of Saskatchewan, which is supported by the Canada Foundation for Innovation (CFI), the Natural Sciences and Engineering Research Council (NSERC), the National Research Council (NRC), the Canadian Institutes of Health Research (CIHR), the Government of Saskatchewan, and the University of Saskatchewan.

■ REFERENCES

(1) Barnum, T. J.; Siebert, M. A.; Lee, K. L. K.; Loomis, R. A.; Changala, P. B.; Charnley, S. B.; Sita, M. L.; Xue, C.; Remijan, A. J.; Burkhardt, A. M.; et al. A Search for Heterocycles in GOTHAM Observations of TMC-1. *J. Phys. Chem. A* **2022**, *126*, 2716−2728.

(2) Charnley, S. B.; Kuan, Y.-J.; Huang, H.-C.; Botta, O.; Butner, H. M.; Cox, N.; Despois, D.; Ehrenfreund, P.; Kisiel, Z.; Lee, Y.-Y.; et al. Astronomical searches for nitrogen heterocycles. *Adv. Space Res.* **2005**, *36*, 137−145.

(3) Etim, E. E.; Adelagun, R. O. A.; Andrew, C.; Enock Oluwole, O. Optimizing the searches for interstellar heterocycles. *Adv. Space Res.* **2021**, *68*, 3508−3520.

(4) Kuan, Y.-J.; Yan, C.-H.; Charnley, S. B.; Kisiel, Z.; Ehrenfreund, P.; Huang, H.-C. A search for interstellar pyrimidine. *Mon. Not. R. Astron. Soc.* **2003**, *345*, 650−656.

(5) Kutner, M. L.; Machnik, D. E.; Tucker, K. D.; Dickman, R. L. Search for interstellar pyrrole and furan. *Astrophys. J.* **1980**, *242*, 541−544.

(6) Bak, B.; Hansen, L.; Rastrup-Andersen, J. Microwave spectra of deuterated furans. Structure of the furan molecule. *Discuss. Faraday Soc.* **1955**, *19*, 30−38.

(7) Barnum, T. J.; Lee, K. L. K.; McGuire, B. A. Chirped-Pulse Fourier Transform Millimeter-Wave Spectroscopy of Furan, Isotopologues, and Vibrational Excited States. *ACS Earth Space Chem.* **2021**, *5*, 2986−2994.

(8) Palmer, M. H.; Wugt Larsen, R.; Hegelund, F. Comparison of theoretical and experimental studies of infrared and microwave spectral data for 5- and 6-membered ring heterocycles: The rotation constants, centrifugal distortion and vibration rotation constants. *J. Mol. Spectrosc.* **2008**, *252*, 60−71.

(9) Sirvetz, M. H. The Microwave Spectrum of Furan. *J. Chem. Phys.* **1951**, *19*, 1609−1610.

(10) Tomasevich, G. R.; Tucker, K. D.; Thaddeus, P. Hyperfine structure of furan. *J. Chem. Phys.* **1973**, *59*, 131−135.

(11) Wlodarczak, G.; Martinache, L.; Demaison, J.; Van Eijck, B. P. The millimeter-wave spectra of furan, pyrrole, and pyridine: Experimental and theoretical determination of the quartic centrifugal distortion constants. *J. Mol. Spectrosc.* **1988**, *127*, 200−208.

(12) Mishra, P.; Hull, A. W.; Barnum, T. J.; McGuire, B. A.; Field, R. W. Chirped-pulse Fourier-transform millimeter-wave rotational spectroscopy of furan in its ν_{10} and ν_{13} excited vibrational states. *J. Mol. Spectrosc.* **2022**, *388*, 111686.

(13) Mellouki, A.; Auwera, J. V.; Demaison, J.; Herman, M. Rotational Analysis of the ν_6 Band in Furan (C_4H_4O). *J. Mol. Spectrosc.* **2001**, *209*, 136−138.

(14) Mellouki, A.; Herman, M.; Demaison, J.; Lemoine, B.; Margulès, L. Rotational Analysis of the ν_7 Band in Furan (C_4H_4O). *J. Mol. Spectrosc.* **1999**, *198*, 348−357.

(15) Tokaryk, D. W.; Culligan, S. D.; Billinghurst, B. E.; van Wijngaarden, J. A. Synchrotron-based far-infrared spectroscopy of furan: Rotational analysis of the ν_{14}, ν_{11}, ν_{18} and ν_{19} vibrational levels. *J. Mol. Spectrosc.* **2011**, *270*, 56−60.
(16) McGuire, B. A.; Burkhardt, A. M.; Kalenskii, S. V.; Shingledecker, C. N.; Remijan, A. J.; Herbst, E.; McCarthy, M. C. Detection of the Aromatic Molecule Benzonitrile (*c*-C_6H_5CN) in the Interstellar Medium. *Science* **2018**, *359*, 202−205.
(17) Cernicharo, J.; Agúndez, M.; Cabezas, C.; Tercero, B.; Marcelino, N.; Pardo, J. R.; de Vicente, P. Pure hydrocarbon cycles in TMC-1: Discovery of ethynyl cyclopropenylidene, cyclopentadiene, and indene. *Astron. Astrophys.* **2021**, *649*, L15.
(18) Doddipatla, S.; Galimova, G. R.; Wei, H.; Thomas, A. M.; He, C.; Yang, Z.; Morozov, A. N.; Shingledecker, C. N.; Mebel, A. M.; Kaiser, R. I. Low-temperature gas-phase formation of indene in the interstellar medium. *Sci. Adv.* **2021**, *7*, eabd4044.
(19) McCarthy, M. C.; McGuire, B. A. Aromatics and Cyclic Molecules in Molecular Clouds: A New Dimension of Interstellar Organic Chemistry. *J. Phys. Chem. A* **2021**, *125*, 3231−3243.
(20) McGuire, B. A.; Loomis, R. A.; Burkhardt, A. M.; Lee, K. L. K.; Shingledecker, C. N.; Charnley, S. B.; Cooke, I. R.; Cordiner, M. A.; Herbst, E.; Kalenskii, S.; et al. Detection of two interstellar polycyclic aromatic hydrocarbons via spectral matched filtering. *Science* **2021**, *371*, 1265−1269.
(21) Sita, M. L.; Changala, P. B.; Xue, C.; Burkhardt, A. M.; Shingledecker, C. N.; Kelvin Lee, K. L.; Loomis, R. A.; Momjian, E.; Siebert, M. A.; Gupta, D.; et al. Discovery of Interstellar 2-Cyanoindene (2-C_9H_7CN) in GOTHAM Observations of TMC-1. *Astrophys. J. Lett.* **2022**, *938*, L12.
(22) Müller, H. S.; Schlöder, F.; Stutzki, J.; Winnewisser, G. The Cologne Database for Molecular Spectroscopy, CDMS: a Useful Tool for Astronomers and Spectroscopists. *J. Mol. Struct.* **2005**, *742*, 215−227.
(23) Müller, H. S. P.; Thorwirth, S.; Roth, D. A.; Winnewisser, G. The Cologne Database for Molecular Spectroscopy, CDMS. *Astron. Astrophys.* **2001**, *370*, L49−L52.
(24) Zdanovskaia, M. A.; Esselman, B. J.; Lau, H. S.; Bates, D. M.; Woods, R. C.; McMahon, R. J.; Kisiel, Z. The 103−360 GHz rotational spectrum of benzonitrile, the first interstellar benzene derivative detected by radioastronomy. *J. Mol. Spectrosc.* **2018**, *351*, 39−48.
(25) Zdanovskaia, M. A.; Martin-Drumel, M.-A.; Kisiel, Z.; Pirali, O.; Esselman, B. J.; Woods, R. C.; McMahon, R. J. The eight lowest-energy vibrational states of benzonitrile: analysis of Coriolis and Darling-Dennison couplings by millimeter-wave and far-infrared spectroscopy. *J. Mol. Spectrosc.* **2022**, *383*, 111568.
(26) Dorman, P. M.; Esselman, B. J.; Park, J. E.; Woods, R. C.; McMahon, R. J. Millimeter-wave spectrum of 4-cyanopyridine in its ground state and lowest-energy vibrationally excited states, ν_{20} and ν_{30}. *J. Mol. Spectrosc.* **2020**, *369*, 111274.
(27) Dorman, P. M.; Esselman, B. J.; Woods, R. C.; McMahon, R. J. An analysis of the rotational ground state and lowest-energy vibrationally excited dyad of 3-cyanopyridine: Low symmetry reveals rich complexity of perturbations, couplings, and interstate transitions. *J. Mol. Spectrosc.* **2020**, *373*, 111373.
(28) Dorman, P. M.; Esselman, B. J.; Woods, R. C.; McMahon, R. J. The 130−500 GHz Rotational Spectrum of 2-Cyanopyridine − Analysis of the Ground Vibrational State and Dyad of Coriolis-Coupled Vibrationally Excited States (in preparation).
(29) Smith, H. H.; Esselman, B. J.; Zdanovskaia, M. A.; Woods, R. C.; McMahon, R. J. The 130-500 GHz Rotational Spectrum of 2-Cyanopyrimidine. *J. Mol. Spectrosc.* **2023**, *391*, 111737.
(30) Esselman, B. J.; Zdanovskaia, M. A.; Smith, H. H.; Woods, R. C.; McMahon, R. J. The 130−500 GHz rotational spectroscopy of cyanopyrazine ($C_4H_3N_2$-CN). *J. Mol. Spectrosc.* **2022**, *389*, 111703.
(31) Simbizi, R.; Nduwimana, D.; Niyoncuti, J.; Cishahayo, P.; Gahungu, G. On the formation of 2- and 3-cyanofurans and their protonated forms in interstellar medium conditions: quantum chemical evidence. *RSC Adv.* **2022**, *12*, 25332−25341.
(32) Amberger, B. K.; Esselman, B. J.; Stanton, J. F.; Woods, R. C.; McMahon, R. J. Precise Equilibrium Structure Determination of Hydrazoic Acid (HN_3) by Millimeter-wave Spectroscopy. *J. Chem. Phys.* **2015**, *143*, 104310.
(33) Esselman, B. J.; Amberger, B. K.; Shutter, J. D.; Daane, M. A.; Stanton, J. F.; Woods, R. C.; McMahon, R. J. Rotational Spectroscopy of Pyridazine and its Isotopologs from 235-360 GHz: Equilibrium Structure and Vibrational Satellites. *J. Chem. Phys.* **2013**, *139*, 224304.
(34) Kisiel, Z.; Pszczółkowski, L.; Drouin, B. J.; Brauer, C. S.; Yu, S.; Pearson, J. C.; Medvedev, I. R.; Fortman, S.; Neese, C. Broadband rotational spectroscopy of acrylonitrile: Vibrational energies from perturbations. *J. Mol. Spectrosc.* **2012**, *280*, 134−144.
(35) Kisiel, Z.; Pszczółkowski, L.; Medvedev, I. R.; Winnewisser, M.; De Lucia, F. C.; Herbst, E. Rotational spectrum of *trans*−*trans* diethyl ether in the ground and three excited vibrational states. *J. Mol. Spectrosc.* **2005**, *233*, 231−243.
(36) Pickett, H. M. The fitting and prediction of vibration-rotation spectra with spin interactions. *J. Mol. Spectrosc.* **1991**, *148*, 371−377.
(37) Kisiel, Z. PROSPE − Programs for ROtational SPEctroscopy, 2023. http://info.ifpan.edu.pl/~kisiel/prospe.htm.
(38) Frisch, M. J.; Trucks, G. W.; Schlegel, H. B.; Scuseria, G. E.; Robb, M. A.; Cheeseman, J. R.; Scalmani, G.; Barone, V.; Petersson, G. A.; Nakatsuji, H., et al. *Gaussian 16*, rev C.01; Gaussian, Inc.: Wallingford, CT, 2016.
(39) Schmidt, J. R.; Polik, W. F. *WebMO Enterprise*, version 19.0; WebMO LLC: Madison, WI, 2019. http://www.webmo.net.
(40) Stanton, J. F.; Gauss, J.; Harding, M. E.; Szalay, P. G.; Auer, R. J.; Bartlett, U.; Benedikt, C.; Berger, D. E.; Bernholdt, Y. J.; Bomble, L.; Cheng, O.; Christiansen, M.; Heckert, O.; Heun, A.et al. Integral packages MOLECULE (J. Almlöf and P. R. Taylor), PROPS (P. R. Taylor), ABACUS (T. Helgaker, H. J. A. Jensen, P. Jørgensen, and J. Olsen), and ECP routines by A. V. Mitin and C. van Wüllen, CFOUR, Coupled-Cluster Techniques for Computational Chemistry, v.2.0, 2014. http://www.cfour.de.
(41) Mills, I. M. Vibration-Rotation Structure in Asymmetric- and Symmetric-Top Molecules. In *Molecular Spectroscopy: Modern Research*; Rao, K. N.; Mathews, C. W., Eds.; Academic Press: New York, 1972; Vol. 1, pp 115−140.
(42) Schneider, W.; Thiel, W. Anharmonic Force Fields from Analytic Second Derivatives: Method and Application to Methyl Bromide. *Chem. Phys. Lett.* **1989**, *157*, 367−373.
(43) Stanton, J. F.; Lopreore, C. L.; Gauss, J. The Equilibrium Structure and Fundamental Vibrational Frequencies of Dioxirane. *J. Chem. Phys.* **1998**, *108*, 7190−7196.
(44) Volka, K.; Adamek, P.; Stibor, I.; Ksandr, Z. Vibrational spectra of 2- and 3-furonitrile. *Spectrochim. Acta, Part A* **1976**, *32*, 397−401.
(45) Smith, H. H.; Kougias, S. M.; Esselman, B. J.; Woods, R. C.; McMahon, R. J. Synthesis, Purification, and Rotational Spectroscopy of 1-Cyanocyclobutene (C_5H_5N). *J. Phys. Chem. A* **2022**, *126*, 1980−1993.
(46) Esselman, B. J.; Kougias, S. M.; Zdanovskaia, M. A.; Woods, R. C.; McMahon, R. J. Synthesis, Purification, and Rotational Spectroscopy of (Cyanomethylene)Cyclopropane-An Isomer of Pyridine. *J. Phys. Chem. A* **2021**, *125*, 5601−5614.

https://doi.org/10.1021/acs.jpca.2c08911
J. Phys. Chem. A 2023, 127, 1909−1922